ACS APPLIED MATERIALS & INTERFACES

RESEARCH ARTICLE

www.acsami.org

Composite Polymeric Magnetic Nanoparticles for Co-Delivery of Hydrophobic and Hydrophilic Anticancer Drugs and MRI Imaging for Cancer Therapy

Abhalaxmi Singh,[†,§] Fahima Dilnawaz,[†,§] Sujeet Mewar,[‡] Uma Sharma,[‡] N. R. Jagannathan,[‡] and Sanjeeb Kumar Sahoo*[,†]

[†]Laboratory of Nanomedicine, Institute of Life Sciences, Nalco Square, Bhubaneswar −751023, Orissa

[‡]Department of NMR & MRI Facility, All India Institute of Medical Sciences, New Delhi-110029

Supporting Information

ABSTRACT: Exercising complementary roles of polymer-coated magnetic nanoparticles for precise drug delivery and image contrast agents has attracted significant attention in biomedical applications. The objective of this study was to prepare and characterize magnetic nanoparticles embedded in polylactide-co-glycolide matrixes (PLGA-MNPs) as a dual drug delivery and imaging system capable of encapsulating both hydrophilic and hydrophobic drugs. PLGA-MNPs were capable of encapsulating both hydrophobic and hydrophilic drugs in a 2:1 ratio. Biocompatibility, cellular uptake, cytotoxicity, membrane potential, and apoptosis were carried out in two different cancer cell lines (MCF-7 and PANC-1). The molecular basis of induction of apoptosis was validated by Western blotting analysis. For targeted delivery of drugs, targeting ligand such as Herceptin was used, and such a conjugated system demonstrated enhanced cellular uptake and an augmented synergistic effect in an *in vitro* system when compared with native drugs. Magnetic resonance imaging was carried out both *in vitro* and *in vivo* to assess the efficacy of PLGA-MNPs as contrast agents. PLGA-MNPs showed a better contrast effect than commercial contrast agents due to higher T_2 relaxivity with a blood circulation half-life ~ 47 min in the rat model. Thus, our results demonstrated the dual usable purpose of formulated PLGA-MNPs toward either, in therapeutics by delivering different hydrophobic or hydrophilic drugs individually or in combination and imaging for cancer therapeutics in the near future.

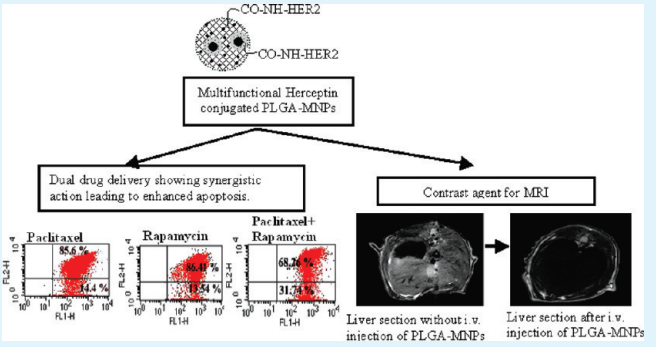

KEYWORDS: polymeric magnetic nanoparticles, sustained release, dual drug delivery, apoptosis, targeted cancer therapy, MRI

1. INTRODUCTION

The application of magnetic nanoparticles (MNP) in the field of biomedical applications such as magnetic drug delivery, magnetic resonance imaging, transfection, and cell and tissue targeting has drawn considerable attention due to MNPs' intrinsic magnetic properties.[1−3] MNPs display superparamagnetism behavior, which permits them to gain magnetism in an applied magnetic field and lose it when the applied field is removed.[4] This property of MNPs is fully exploited when they are used as drug delivery agents, wherein chemotherapeutic drugs can be targeted to the desired specific location in the body by application of an external magnetic field. As a consequence, they reduce the systemic side effects[5] by lowering the collateral toxic effects on the healthy cells or tissues.[6] Apart from that, currently, significant attention has been paid to the multifunctional characteristics and complementary role of MNPs as a contrast agent for magnetic resonance imaging (MRI).[7−9] Though sometimes the contrast difference between the considered biological tissues is trivial, with the aid of an efficient contrast agent, it is fairly possible to offer higher contrast and information-rich images for disease detection. Although different commercial contrast agents like Resovist and Feridex IV are available on the market, the problems faced with using them include poor cellular uptake and failure to provide a high contrast signal.[10] In addition, these agents could not be used as a dual efficient system for drug delivery and imaging.[10] Thus, for real time monitoring of drug distribution in targeted tissues, the imaging enhancement property of the magnetic nanoparticles could be implemented with the application of drug delivery.

For effective tumor therapy, prolonged availability of the drug at the target site is the primary requisite of any drug delivery system. In this regard, drug retention and drug release properties are indispensable features which should be taken into consideration. Embedding magnetic nanoparticles into supplementary sustained release polymeric systems such as poly dl-lactide-co-glycolide (PLGA), polylactides (PLL), or polylactic acid (PLA) or in dendrimer matrixes

Received: December 6, 2010
Accepted: February 16, 2011
Published: March 03, 2011

has boosted the delivery of drugs to the target sites by increasing drug efficiency and maximizing the drug retention option at the target site.[11−15] These blending components of polymeric magnetic nanoparticles act as a shell or reservoir to carry the drug component for therapeutic purposes, whereas the constituent of magnetite makes carriers possible for applications like MRI, thus endowing the MNPs with dual properties.

One of the promising approaches of the drug delivery system is the co-delivery of different drugs using the same delivery vehicle for the treatment of cancer[16−18] with the potential advantage of a synergistic effect,[19] suppressed drug resistance,[20] and the ability to tune the drug dosage. One of the main challenges of combined therapy is to control the release behavior of each drug independently. However, very little work has been done on magnetic nanoparticles that have been used as dual drug delivery systems. In our previous work, we encapsulated two hydrophobic drugs, i.e., paclitaxel and rapamycin, in our magnetic nanoparticle formulation.[21] Similarly, Jain et al. have also used MNPs to deliver two hydrophobic drugs, i.e., doxorubicin and paclitaxel.[22] Here, we have tried to encapsulate hydrophobic and hydrophilic drugs simultaneously in a proper ratio in our magnetic nanoparticle formulation. However, several attempts were taken to encapsulate both hydrophilic and hydrophobic drugs together inside different polymeric nanoparticles, but, of note, a synergistic effect was not observed due to the disproportion of the drug ratios.[18,23] Recently, in 2010, Aryal et al. prepared drug conjugates of paclitaxel and gemcitabin which significantly improved the cytotoxicity of free drugs.[24] Yang et al. investigated the synthesis and release characteristics of poly(ethyl-2-cyanoacrylate) (PECA) coated magnetite nanoparticles containing hydrophobic and hydrophilic anticancer agents[25] but could not achieve a proper therapeutic ratio, which could show a synergistic drug effect. Therefore, a proper ratio of two different hydrophobic and hydrophilic drugs in the magnetic polymeric system is necessary to bring a notable synergistic effect.

Herein, we report a magnetic polymeric delivery system as a model carrier that can deliver/co-deliver hydrophobic or hydrophilic drugs alone or in combination. For this, we synthesized and characterized various drug-loaded PLGA-MNPs containing the hydrophobic (paclitaxel, rapamycin) and hydrophilic (carboplatin) drugs alone or in combination for cancer treatment. Unique molecular signatures found on the malignant cells facilitate selective targeting of cancer cells more efficiently. In this regard, monoclonal antibodies (mAbs) were exploited for targeted delivery of MNPs[26,27] due to their high specificity. Recently, the development of Herceptin, an FDA-approved mAb to the HER2/neu (erbB2) receptor, has made it a popular targeting agent for nanoparticles.[28] Therefore, with the intention of active targeting, the specific ligand herceptin was conjugated to drug-loaded PLGA-MNPs. The *in vitro* efficacy of such conjugated systems as therapeutic agents was validated using model breast cancer (MCF-7) and pancreatic cancer cell lines (PANC-1) in different techniques. Moreover, the diagnostic potential of these MNPs as MRI probes was studied both *in vitro* and *in vivo*. Thus, our approach clearly indicates the simultaneous use of MNPs as targeted dual drug delivery and imaging agents, providing the scope of not only delivering therapeutic agents at the diseased site but also monitoring the drug distribution in tissue to further evaluate the response of the therapy.

2. EXPERIMENTAL SECTION

2.1. Materials. Pure granulated 99% iron(III) chloride hexahydrate ($FeCl_3 \cdot 6H_2O$), 99% iron(II) chloride tetrahydrate ($FeCl_2 \cdot 4H_2O$), carboplatin, 6-coumarin, MTT (3-(4, 5-dimethylthiazol-2-yl)-2, 5-diphenyl tetrasodium bromide) reagent, JC-1 dye, and the Annexin V FITC apoptosis kit were purchased from Sigma-Aldrich (St. Louis, MO). Glyceryl monooleate (GMO) was procured from Eastman (Memphis, TN). Poly(D,L-lactide-co-glycolide) (PLGA) (polylactide/glycolide = 65:35, molecular weight = 97 000 Da, density = 0.55−0.75 dL/g) was purchased from Birmingham Polymers, Inc. (Birmingham, USA). Polyvinyl alcohol (PVA, average MW 30 000−70 000) was purchased from Sigma Aldrich Co. (St Louis, MO). N-(3-Dimethylaminopropyl)-N′-ethyl-carbodiimide hydrochloride (EDC) and N-hydroxy succinimide (NHS) were procured from Fluka and Sigma Aldrich, Belgium. Paclitaxel and rapamycin were obtained from Shaanxi Schiphar Biotech Pvt Ltd., China. HER2 was purchased from Roche, USA. Primary antibodies for PARP-1/p-γ-H2AX/p53/p21 and β actin and the secondary antibodies against them were purchased from Santacruz Biotechnology, Santacruz, California. The primary antibody for p70S6K1 was purchased from Imgenex Corporation, San Diego. All other chemicals used were of analytical grade obtained from Sigma (St. Louis, MO). Milli Q water purged with nitrogen (N_2) gas was used in all steps involved in the synthesis and formulation of magnetic nanoparticles.

2.2. Synthesis of Drug-Loaded PLGA-MNPs. Initially, the synthesis of glyceryl monooleate coated Fe_3O_4 particles was performed following our previous protocol.[21] The PLGA-MNPs were formulated using the double emulsion (W/O/W) method.[29] To synthesize the void PLGA-MNPs, 100 mg of GMO-MNPs was dispersed in 1 mL of Milli Q water and sonicated using a microtip sonicator set at 55 W of energy output for 30 s (VC505, Sonics Vibracell, Sonics and Materials Inc., Newtown, USA) in an ice bath. A total of 100 mg of PLGA was dissolved in 2 mL of dichloromethane (DCM), and to this the GMO-MNP dispersion was added dropwise and vortexed for 5 min to get the primary water in oil emulsion. Next, 4 mL of 5% PVA (w/v) was added to the mixture and sonicated for 30 s in an ice bath for stabilization of the emulsion. The resulted double emulsion (water in oil in water) was finally diluted with 30 mL of 1% PVA (w/v) and stirred for 3 h to evaporate the organic solvent at room temperature. Then, it was washed three times with N_2 purged Milli Q water at 20 000 rpm for 20 min at 10 °C (Sigma centrifuge, 3-16PK, Osterode, Germany).

For the incorporation of anticancer drugs in PLGA-MNPs, hydrophobic drugs such as paclitaxel and rapamycin and hydrophilic drugs like carboplatin were used. For combined drug formulation, paclitaxel + rapamycin and paclitaxel + carboplatin were considered. In brief, to prepare the hydrophobic drug-loaded PLGA-MNPs, during the emulsification process, 10 mg of the drug was added to the PLGA dissolved in DCM for individual drug formulation before making the primary emulsion; however, for the combined drug formulation, 5 mg of paclitaxel and 5 mg of rapamycin was added. But, for hydrophilic drug incorporation, 10 mg of carboplatin was dissolved in 500 μL of water and added to the GMO-MNP dispersion in water before proceeding toward the primary emulsion. For the dual drug formulation of hydrophobic and hydrophilic drugs paclitaxel + carboplatin, 5 mg of carboplatin, dissolved in 250 μL of water, was added to the GMO-MNP dispersed in water, and 5 mg of paclitaxel was added to the PLGA dissolved in a DCM solution during the emulsification process.

To determine the cellular uptake of the drug-loaded PLGA-MNPs, fluorescent dye 6-coumarin was taken as a model fluorescent probe. Even at an acidic pH, the dye remains associated with the nanoparticles, as proven earlier, and offers a sensitive method to quantitatively determine their intracellular uptake and retention.[30−32] To formulate 6-coumarin-loaded PLGA-MNPs, 50 μL of the 6-coumarin dye dissolved in methanol/chloroform (12.5: 87.5 v/v; 1 mg/mL) was added to the PLGA dissolved in a DCM solution prior to emulsification instead of drugs in the formulation.

2.3. Physical Characterization of Nanoparticles. The physical characterization of formulated PLGA-MNPs was done by measuring the particle size and ζ potential using a particle size analyzer, the internal

structure by TEM measurement, the surface morphology by SEM measurement, the crystallographic structure by XRD analysis, the magnetization study by using SQUID, the thermal stability by thermogravimetric analysis, the physical state analysis of drugs in PLGA-MNPs by differential scanning calorimetry, and probable chemical interactions of iron oxide, drugs, and polymers in the PLGA-MNP formulations were carried out using FT-IR spectra. Quantification of the drug incorporated in the PLGA-MNPs and its release from the PLGA-MNPs was carried out through RP-HPLC (all of the details of the protocol are in the Supporting Information).

2.4. Formulation of HER2-PLGA-MNPs and Uptake Study. To the drug-loaded PLGA-MNPs, antibody HER2 was conjugated using the chemical conjugation method.[21,30] In brief, 10 mg of void or drug-loaded PLGA-MNPs was added to 5 mL of PBS (0.02 M, pH 7.4), to which 250 μg of EDC and 250 μg of NHS was added. The sample was stirred at room temperature for 4 h and then magnetically decanted to remove free EDC and NHS. To the pellet, 3 mL of PBS (0.02 M, pH 7.4) and 100 μL of HER2 (1 mg/mL) was added. The solution was left for 2 h under magnetic stirring and then incubated at 4 °C overnight. The next day, magnetic decantation was done, and the pellet was washed three times with PBS (0.02 M, pH 7.4) to remove unconjugated antibodies. The same protocol was used for the conjugation of HER2 to the 6-coumarin-loaded PLGA-MNPs for the uptake studies. The cellular uptake efficiency of PLGA-MNPs and HER2 conjugated PLGA-MNPs was determined by MNP assay and a fluorescence study, both quantitatively and qualitatively (Supporting Information).

2.5. PLGA-MNPs for Imaging. *2.5.1. Preparation and Relaxation Measurement of Magnetic Nanoparticles in Phantom Gels.* Different concentration ranges of 0−50 μg/mL of PLGA-MNPs and different drug-loaded PLGA-MNPs were prepared in PBS (0.1 M, pH 7.4). A 2.5% w/v agar solution was prepared by heating 500 mg of agar in 20 mL of PBS at 80 °C for 10 min. For preparing phantom gels, 320 μL of the agar solution was mixed with 1680 μL of a PLGA-MNP suspension at each concentration and was preheated to avoid gelation while mixing. Tubes containing MNPs in gel were positioned in a Bruker Biospec 4.7 T MRI Scanner (BIOSPEC Bruker BioSpin MRI GmbH, Germany) using a 72 mm resonator as a transmitter/receiver coil. To estimate the transverse relaxation time (T_2) for each sample, coronal images (slice thickness = 2 min) were acquired at various echo times (TE) from 20 to 320 ms with a repetition time (TR) of 10 000 ms. Similarly, the T_1 relaxation time for each sample was measured by varying TR between 15.4 ms and 10 000 ms while keeping TE constant at 10 ms. MR signal intensity was calculated by drawing uniform circular ROIs (0.26 cm^2).

2.5.2. Determination of Blood Circulation Half-Life. The half-life of PLGA-MNPs in blood was determined after intravenous injection (dose, 7 mg PLGA-MNPs/kg body weight) into the Wistar rats (male, ∼250 g, three per experiment). Blood samples (∼300 μL) were drawn from the tail vein before injection and at different time intervals up to 90 min post injection. To determine the T_2 relaxivity in MRI, the blood samples were four-times diluted in PBS (0.01 M, pH 7.4), and the phantom images were taken and the signal intensities calculated in a manner the same as that for the phantom agar gel.[22] The relative concentration of PLGA-MNPs was estimated from the signal intensity changes using the following equation:[22]

$$[\text{PLGA-MNP}]\alpha - \ln[S(t)/S_0]$$

where S_0 is the signal intensity before injection and $S(t)$ is the signal intensity of PLGA-MNPs at time t post injection.

2.5.3. In Vivo MRI. To test the utility of the PLGA-MNPs as contrast agents for MRI, a blood clearance study and MRI imaging of rats before and after injecting PLGA-MNPs at different time intervals were studied. MR experiments were carried out at 4.7 T (BIOSPEC Bruker BioSpin MRI GmbH, Germany) using a 72 mm resonator as a transmitter/receiver coil. The Institutional Animal Ethics Committee approved the study. During MR experiments, animals were anesthetized using isofluorane inhalation anesthesia given along with oxygen. Initially, a concentration of 3% isofluorane (given for 1 min) was used to immobilize rats using a vaporizer for the fluorane anesthetic (Model 100 Vaporizer, Surgivet). Following the fixation of the rat to the animal bed, the concentration was reduced to 1.5%, which was maintained throughout the duration of the MR experiment. The body temperature was maintained constant during the experiment using a circulating warm water bath attached to the animal bed. Wistar rats (male, ∼250 g, two per experiment) were injected with a suspension of PLGA-MNPs (dose, 7 mg PLGA-MNPs/kg body weight) diluted in a mannitol−citrate isotonic solution. The rats were injected via the saphenous vein using a 30 gauge heparinized needle with an infusion time of 30 s.

Following scout images in all three planes, T_2-weighed (T_2-W) images using the RARE sequence were acquired in axial planes using the following parameters: TR/TE = 2000/41.1 ms, RARE factor = 8, slice thickness = 2 mm, inter slice distance = 2 mm, average = 9, and matrix size = 256 × 256.

Intensities were calculated in control and treated rats at various time intervals up to 48 h by drawing uniform circular ROIs (0.26 cm^2).

2.6. Antiproliferative Assay. To find the cytotoxicity of different formulations, a cytotoxicity assay was carried out in two different cell lines (MCF-7 and PANC-1).[21] The cells were seeded at 2500 per well in a 96-well plate (Corning, NY) and kept overnight in the incubator (Hera Cell, Thermo Scientific, Waltham, MA) for cell attachment. Different concentrations of the drug individually or in a combination of forms (drug concentration, 1 ng/mL to 10 μg/mL), either in solution or loaded in PLGA-MNPs, or HER2 conjugated PLGA-MNPs were added to the MCF-7 and PANC-1 cells. Cells treated with void PLGA-MNPs and cells treated with only media were used as respective controls. The medium was changed on the second and fourth days following the drug treatment; no further dose of the drug was added. The viability of the cells was determined on the fifth day. After the specified incubation time, 10 μL of MTT (5 mg/mL) was added, and the plates were incubated for 3 h at 37 °C in a cell culture incubator. The percentage of cell viability relative to untreated controls was determined on the basis of the mitochondrial conversion of yellow MTT, a tetrazole, to purple formazan by the living cells.[33] The formazan crystals were solubilized in dimethyl sulfoxide, and the color intensity was measured at 540 nm using a microplate reader (Synergy HT, BioTek Instruments, Inc., Winooski, VT). The antiproliferative effect of different treatments was calculated as a percentage of cell growth with respect to respective controls.

2.7. Measurement of Mitochondrial Membrane Potential. A decrease in the mitochondrial membrane potential is one of the characteristic features of the apoptotic pathway. So, to know the effect of different drug formulations on the cells for conferring the apoptotic pathway, a mitochondrial membrane depolarization study was done in both MCF-7 and PANC-1 cell lines by using flow cytometry.[34] Briefly, 5 × 10^5 cells were grown in 25 cm^2 culture flasks (BD Biosciences, CA, USA) containing 5 mL of media and allowed to attach overnight in the incubator at 37 °C. The cells were exposed to a particular concentration (0.1 μg/mL) of the native drug, drug-loaded PLGA-MNPs, and the HER2 conjugated drug-loaded PLGA-MNPs and incubated at 37 °C for 24 h. The next day, the cells were washed three times with PBS (0.1 M. pH, 7.4). Then, the cells were resuspended with 1 mL of PBS (0.1 M pH, 7.4), and the cationic dye JC-1 (3 μg/mL) was added and incubated for 10 min at 37 °C to allow a potential-dependent accumulation of the dye in mitochondria. The cells were washed with PBS (0.1 M, pH 7.4) twice and analyzed by using a FACScan flow cytometer and Cell Quest Caliber software (Becton-Dickinson, CA). All experiments were performed in triplicate. To know the detailed division of apoptotic cell population at diverse stages, an apoptosis study using Annexin V-FITC and propidium iodide dye by flow cytometry was carried out (Supporting Information)

2.8. Western Blotting. To study the molecular mechanism of the apoptosis initiated by different drug-loaded PLGA-MNP formulations, a

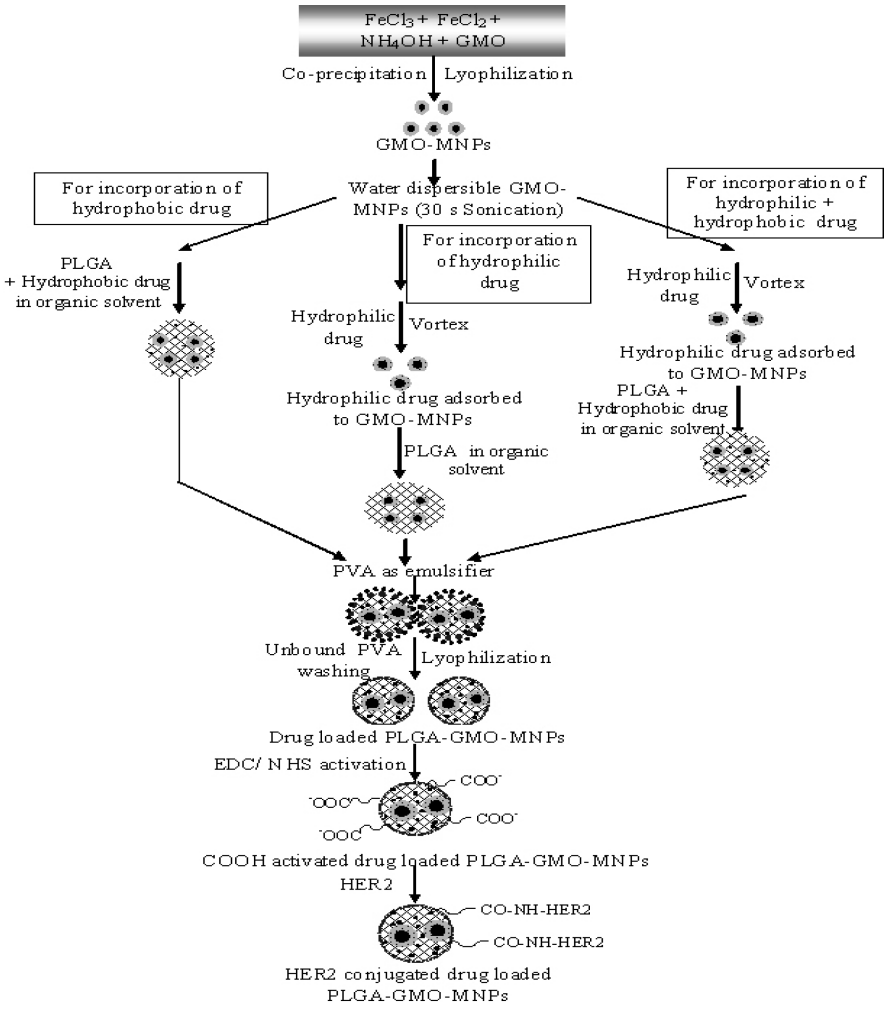

Figure 1. Schematic representation of the formulation of different HER2 conjugated drug-loaded PLGA-MNPs.

Western blot analysis was performed.[30] In brief, 5×10^5 MCF-7 cells/mL were grown in 25 cm^2 culture flasks (BD Biosciences, CA) and allowed to attach overnight at 37 °C. The next day, the media were replaced with fresh media containing a 0.1 μg/mL concentration of the native drug (paclitaxel/rapamycin/carboplatin, paclitaxel + rapamycin/paclitaxel + carboplatin), drug-loaded PLGA-MNPs, and HER2 conjugated drug-loaded PLGA-MNPs and were incubated for 24 h. The next day, cells were washed with cold PBS (0.01 M, pH 7) and lysed in a lysis buffer containing 50 mmol/L of Tris-HCl (pH 8.0), 150 mmol/L of NaCl, 1% NP40, 0.5% Na-deoxycholate, and 0.1% SDS, containing protease and a phosphatase inhibitor (Sigma, St. Louis, MO). The protein concentration in the cell lysate was determined with a micro-BCA protein assay (Pierce, Rockford, IL). Protein lysates containing 60 μg of the protein were separated by 10% SDS-PAGE and transferred to a PVDF membrane. Then, the membrane was blocked with 5% blocking solution and incubated with primary antibodies against PARP-1/p-γ-H2AX/p53/p21/ β actin and p70S6K1 in a 1:1000 dilution for 1 h at room temperature and an HRP conjugated secondary antibody (1:5000 dilution) for 40 min at room temperature. The immunoblots were visualized using the enhanced chemiluminescence detection kit (ECL; Amersham, Arlington Heights, IL).

2.9. Cell Culture. The cell culture experiments were carried out in the MCF-7 (breast cancer) and PANC-1 (pancreatic cancer) cell lines purchased from American Type Culture Collection (Manassas, VA). The cells were grown in a DMEM medium supplemented with 10% fetal bovine serum, 100 μg/mL of penicillin G, and 100 μg/mL of streptomycin at 37 °C in a humidified and 5% CO_2 atmosphere maintained in an incubator (Hera Cell, Thermo Scientific, Waltham, MA). All of the chemicals pertaining to the cell culture were purchased from Himedia Laboratories Pvt. Ltd., Mumbai, India.

2.10. Statistical Analysis. Statistical analyses were performed using Student's *t* test. The differences were considered significant for *p* values of <0.05.

3. RESULTS

3.1. Physicochemical Characterization of Different PLGA-MNP Formulations. Our previous study mentioned about the aqueous dispersibility of synthesized GMO-MNP.[21] However, drug loaded PLGA coated GMO-MNPs were prepared through double emulsion solvent evaporation method (Figure 1). The amphiphilic nature of the GMO allocates the residence of the hydrophilic drug to adhere to its surface during the formulation process, where as the hydrophobic drugs like paclitaxel and rapamycin were distributed in the PLGA polymer matrix apart from adhering to the GMO coating. The emulsifier PVA was used to stabilize the nanoformulation. Dynamic light scattering analysis revealed the hydrodynamic diameter of the various formulated nanoparticles in the range of 240 - 310 nm with polydispersity index ~0.2 of different formulations depicted very narrow size distribution of the nanoparticles.

Table 1. Physical Characterization of Hydrophobic and Hydrophilic Drug-Loaded PLGA-MNPs

sample	size (nm) ± SD[a]	ζ potential (mV) ± SD[b]	polydispersity index ± SD[c]	encapsulation efficiency (%) ± SD[d]
PLGA-MNP	240 ± 7.7	−23.2 ± 3.1	0.2 ± 0.03	
Pac- PLGA-MNP	270 ± 4.5	−18.07 ± 2.1	0.27 ± 0.01	82.2 ± 2.1
Rapa- PLGA-MNP	265 ± 6.2	−19.02 ± 3.3	0.1 ± 0.03	84.3 ± 2.3
Carbo- PLGA-MNP	281 ± 5.5	−17.3 ± 3.4	0.31 ± 0.02	47.7 ± 1.1
Pac+rapa- PLGA-MNP	304 ± 4.1	−18.65 ± 2.9	0.22 ± 0.04	Pac 80.6 ± 2.7 Rapa 86.6 ± 3.1
Pac+carbo- PLGA-MNP	310 ± 3.9	−19.17 ± 2.6	0.26 ± 0.03	Pac 83.5 ± 3.0 Carbo 47.8 ± 1.5

[a] Size in nanometers as measured by dynamic laser scattering method. [b] ζ potential in millivolts as measured by a zeta sizer. [c] Polydispersity index as measured by a zeta sizer. [d] Encapsulation efficiency of the different drugs in PLGA-MNPs as measured by RP-HPLC.

The void PLGA-MNPs have a diameter of 263 nm; after encapsulation of the drug in the PLGA-MNPs, the particle size increased due to incorporation of the drugs, either single or in combination.[35]

The stability of the particulate system principally depends on the ζ potential and surface charge of the nanoparticles, because it directly affects the physical stability, cellular uptake, biodistribution, and drug release from the nanoparticles.[30] The ζ potential measurement of the void PLGA-MNPs showed a high negative ζ potential of about −23 mV. The negative ζ potential is attributed to the presence of a carboxylic group in the PLGA polymer.[35] The ζ potential values decreased slightly with the encapsulation of the drug in PLGA-MNPs (Table 1). Thus, a high ζ potential of the formulated particles helps them to repel each other and prevent aggregation.[23]

TEM images revealed that GMO-MNPs were of a diameter of ∼7 nm (Figure 2a), whereas the formulated PLGA-MNPs showed an internal diameter of ∼100 nm (Figure 2b). From the images, it was observed that, after encapsulation, the GMO-MNPs get entrapped and remain scattered inside the polymer matrix (Figure 2b). Similar results were also observed by Kim et al., and the particle size was found to be 100−200 nm.[36] The size distribution pattern from the TEM images revealed a narrow range of distribution of the particles from ∼90 to 120 nm having a mode diameter value of 100 nm (Figure 2c). The particle size measurement by laser light scattering was higher than that of TEM measurement, because it provides information on the hydrodynamic layers formed due to the hydrophilic coating around the cluster of PLGA-MNPs.[30] Previously, it was explained by Probha et al. that the PVA associated with nanoparticles could contribute to forming layers of aggregates around the surface of nanoparticles contributing to the hydrodynamic size.[37] The surface morphology of the PLGA-MNPs observed through SEM revealed spherical and smoothed topology (Figure 2d). The crystallographic structure and chemical composition of formulated PLGA-MNPs was revealed from the XRD analysis. The X -ray diffraction pattern of the PLGA-MNPs revealed the diffractional peaks at (111), (220), (311), (400), (422), and (511), which are the characteristic peaks of a Fe_3O_4 crystal with a cubic spinel structure.[38] The position and the relative intensity of all diffraction peaks were identical with standard spectra of the bulk magnetite. Similar peaks for the Fe_3O_4 crystal were observed after coating the MNPs with PLGA by Liu et al.[39] However, no peaks corresponding to γ-Fe_2O_3 and α-Fe_2O_3 like 210, 213, etc. were observed, suggesting the purity of MNPs. This suggests that even after the PLGA coating, the purity of the Fe_3O_4 has been maintained (Figure 2e).

The SQUID analysis of the PLGA-MNPs showed typical hysteresis curves at 300 K (Figure 3a) having negligible coercivity at room temperature, and the saturation magnetism was around 29 emu/g. The magnetization curves intersect with the zero point and overlap, explaining the fact that the remaining magnetization was zero in the absence of the external magnetic field. The hysteresis loop had negligible coercivity at room temperature, and the magnetization at 1.5 T (after subtracting the diamagnetic background) was 53.5 ± 0.7 emu/g for GMO-MNPs and 66.0 ± 0.3 emu/g for uncoated MNPs at 300 K. After coating with PLGA, the magnetization value decreased to 29 ± 0.4 emu/g. The saturation magnetization of the formulated GMO-MNPs, i.e., *Ms* at 10 and 300 K, and the coercivity *Hc* of native MNPs and GMO-MNPs are shown in Table 2.

A TGA analysis was performed to determine the precise weight loss/gain of the formulated compound as a function of the temperature. It is based on the mass loss of individual components. Figure 3b depicts the thermograms of native iron oxide particles, pure GMO, GMO-MNPs, and PLGA-MNPs. Pure GMO showed a mass loss at about 200 °C, but coated GMO-MNPs illustrated a 10% mass loss at about 500 °C, reflecting the chemisorption of GMO on MNP surfaces.[21] However, the PLGA-MNPs demonstrated a 50% mass loss after 200 °C. This information confirmed that the formulated PLGA-MNPs contained about 50% of PLGA by mass, implying that the remaining 50% of the nanoparticles are contributed by GMO-MNPs. After drug loading, there was no substantial difference in weight loss of PLGA-MNPs (data not shown).

3.2. Entrapment Efficiency of Different Drugs in PLGA-MNPs. The successful implementation of a high payload of the drug inside the nanoparticulate formulations reduces the quantity of the nanoparticle required for administration. In our formulation, a high payload of both hydrophobic and hydrophilic drugs could be achieved. Hydrophobic drugs such as paclitaxel and rapamycin and hydrophilic drug carboplatin were successfully encapsulated either alone or in combination. The quantitative estimation through RP-HPLC revealed that with 5% (w/w) drug loading, the encapsulation efficiency of the hydrophobic drugs either alone or in combination (paclitaxel + rapamycin) showed a higher drug entrapment of ∼80% (i.e., ∼80% of the added drug was entrapped in the formulation); on the other hand, the hydrophilic drug carboplatin showed a drug entrapment of ∼47% (i.e., ∼47% of the added drug was entrapped in the formulation) alone and in the combination form (with paclitaxel), as depicted in Table 1. The possible chemical interaction that had occurred between different drugs within PLGA-MNPs was exemplified by FT-IR analysis (Supporting Information, Figure S2).

3.3. Physical Status of Drug by DSC. Through DSC analysis, the possible chemical interaction and the physical state of drug inside the PLGA-MNPs could be detected. The presence of a crystalline structure of the drug might affect the release of the

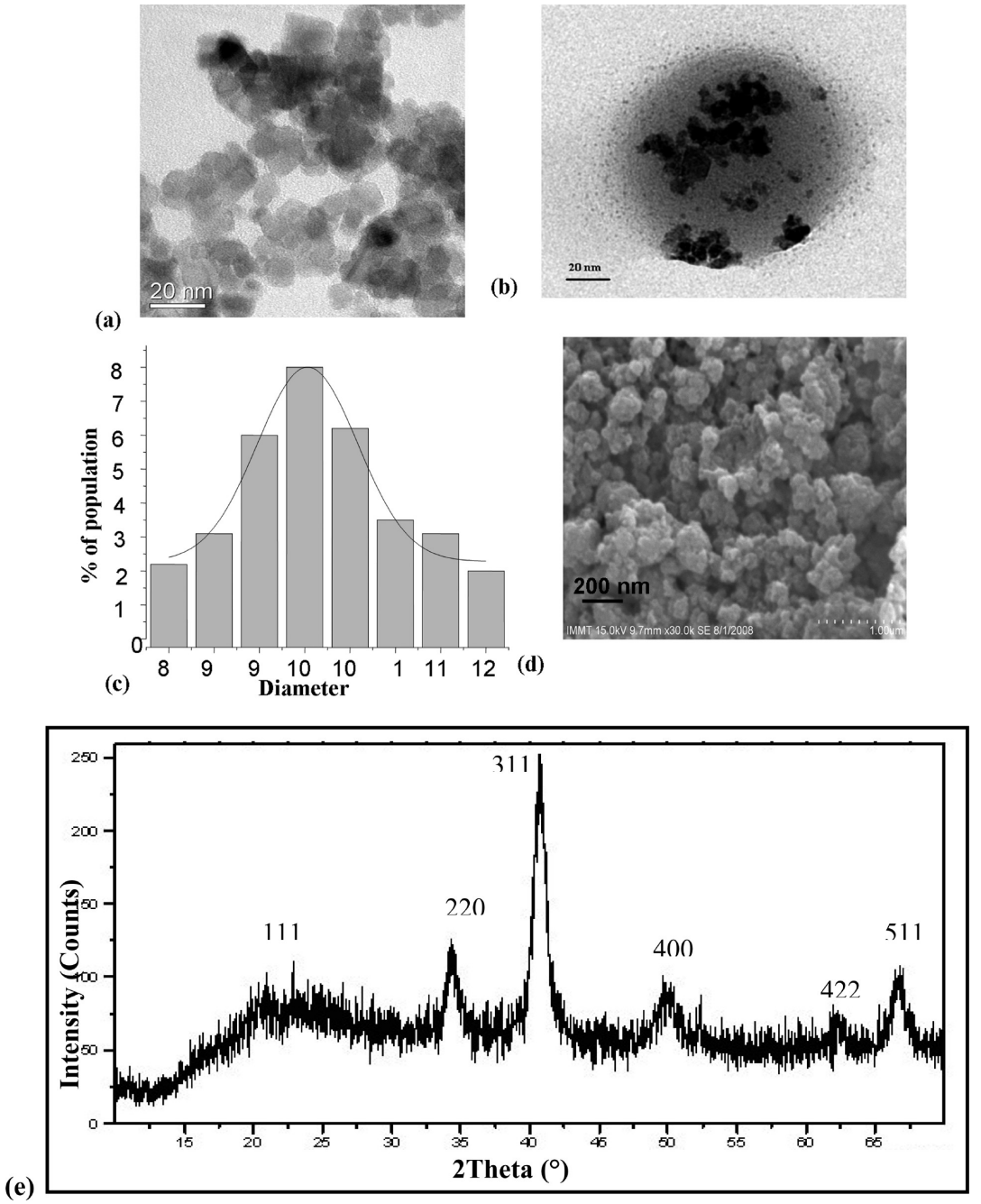

Figure 2. (a) TEM of GMO- MNP, (b) TEM of PLGA-MNPs, (c) particle size distribution of PLGA-MNPs measured by TEM (average values of 20 measurements), (d) SEM of PLGA-MNPs, and (e) XRD powder pattern of PLGA-MNPs.

drug from the PLGA-MNP formulations. Thus, it is essential to know the physical state of the drug inside the PLGA-MNPs. Native paclitaxel has an endothermic peak at 215 °C (Figure 3c. i). The paclitaxel loaded PLGA-MNPs (Figure 3c.iv) do not show any such peaks. Similarly, native rapamycin (Figure 3c.ii) has an endothermic peak at 180 °C which cannot be visible in the rapamycin loaded nanoparticles (Figure 3c.v). These paclitaxel and rapamycin peaks also cannot be found in the combined (paclitaxel + rapamycin) formulation (Figure 3c.vi). This absence of specific peaks for the crystalline domain of the native drug suggests that the drugs inside the PLGA-MNPs are in an amorphous state or disordered-crystalline state or in a solid-state solubilized form.[40] In addition, native carboplatin (Figure 3d.i) has an endothermic peak at around 270 °C which is not visible in carboplatin loaded nanoparticles (Figure 3d.iii) and also in combined (paclitaxel + carboplatin) drug formulation (Figure 3d.iv). This suggests that in all of the drug-loaded PLGA-MNP formulations, the drug is present in an amorphous or distorted crystalline structure, which will help the drug to be released from the nanoformulations in a sustained manner. The PLGA has a glass transition temperature at 54 °C which can be visible in the void PLGA-MNPs and also in the drug-loaded PLGA-MNPs (Figure 3c.iii and d.ii).

3.4. MRI Characteristic of PLGA-MNPs. The phantom magnetic resonance imaging experiments were carried out to evaluate the detectability of the formulated void PLGA-MNPs. The

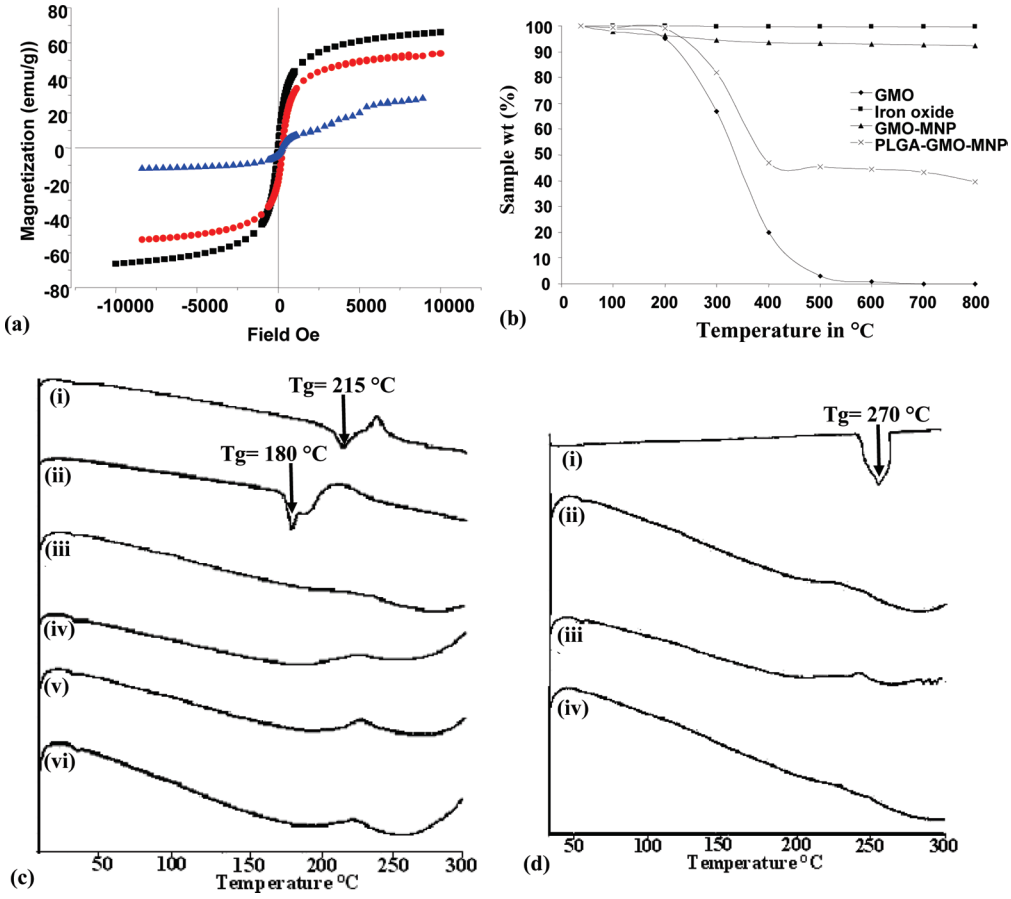

Figure 3. (a) Magnetization curve of MNP (■), GMO-MNP (●), and PLGA-MNP (▲) as a function of the field measured at 300 K. (b) Thermogravimetric analysis (TGA) of GMO (♦), native iron oxide (■), GMO-MNPs (▲), and PLGA-MNPs (×). (c) Differential scanning calorimetry (DSC) curves of (i) native paclitaxel, (ii) native rapamycin, (iii) void PLGA-MNPs, (iv) Pac-PLGA-MNPs, (v) Rapa-PLGA-MNPs, and (vi) Pac+Rapa-PLGA-MNPs. (d) Differential scanning calorimetry (DSC) curves of (i) native carboplatin, (ii) void PLGA-MNPs, (iii) Carbo-PLGA-MNPs, and (iv) Pac+Carbo-PLGA-MNPs.

Table 2. Effect of GMO on Magnetic Properties of Iron Oxide Nanoparticles

samples	saturation magnetization *Ms* (emu/g) at 10 K ± SD	saturation magnetization *Ms* (emu/g) at 300 K ± SD	coercive field *Hc* (Oe)
native iron oxide (MNP)	57 ± 0.4	66 ± 0.3	349.89
GMO-MNP	55 ± 0.4	53 ± 0.7	349.98
PLGA-MNP	24 ± 0.6	29 ± 0.4	249.72

transverse relaxation time T_2 was observed to be reduced in different MNP concentrations (measured in micrograms of Fe per milliliter) of the phantom gels compared to the control gel (Figure 4a). In addition, with an increase in the particle concentration of PLGA-MNPs from 0.1 μg/mL to 50 μg/mL, the reduction of T_2 was more significant, which is evident from the decrease in the signal intensity (Figure 4b). Also, with an increasing concentration of PLGA-MNPs, enhancement of the relaxation rate R_2 ($R_2 = 1/T_2$) can be observed (Figure 4c).

3.5. *In Vitro* Imaging of PLGA-MNPs after Drug Loading. The imaging characteristics of various drug-loaded PLGA-MNPs were evaluated in a phantom gel. In the drug-loaded PLGA-MNPs, the relaxation rate R_2 increased with an increase in the concentration of the drug-loaded PLGA-MNPs, as was observed in the case of void PLGA-MNPs. However, the R_2 of drug-loaded PLGA-MNPs was comparatively less than that of the void PLGA-MNPs. The calculated relaxivity was in the following order of arrangement: void PLGA-MNP > Pac-PLGA-MNP ~ Rapa-PLGA-MNP > Carbo-PLGA-MNP. Between the two hydrophobic drug-loaded (paclitaxel, rapamycin) PLGA-MNPs, no significant change in the T_2 relaxivity rate was observed. On the other hand, the hydrophilic carboplatin-loaded PLGA-MNPs showed the lowest T_2 relaxivity among all of the drug-loaded formulations (Figure 4c).

3.6. Evaluation of Circulation Half-Life of PLGA-MNPs *in Vivo*. The PLGA-MNPs' half-life in blood was determined after intravenous injection in a rat model. The blood samples were drawn from the tail vein of the rats at different time intervals (post injection, 30 min, 1 h, 2 h, 4 h, 24h, and 48 h), and the corresponding phantom gels were prepared and analyzed to determine the change in signal intensity. Post injection, there was a reduction in signal intensity, followed by minor alteration of the signal intensity up to 45 min. Subsequently, there was a sudden increase in signal intensity. The half-life of the PLGA-MNPs in

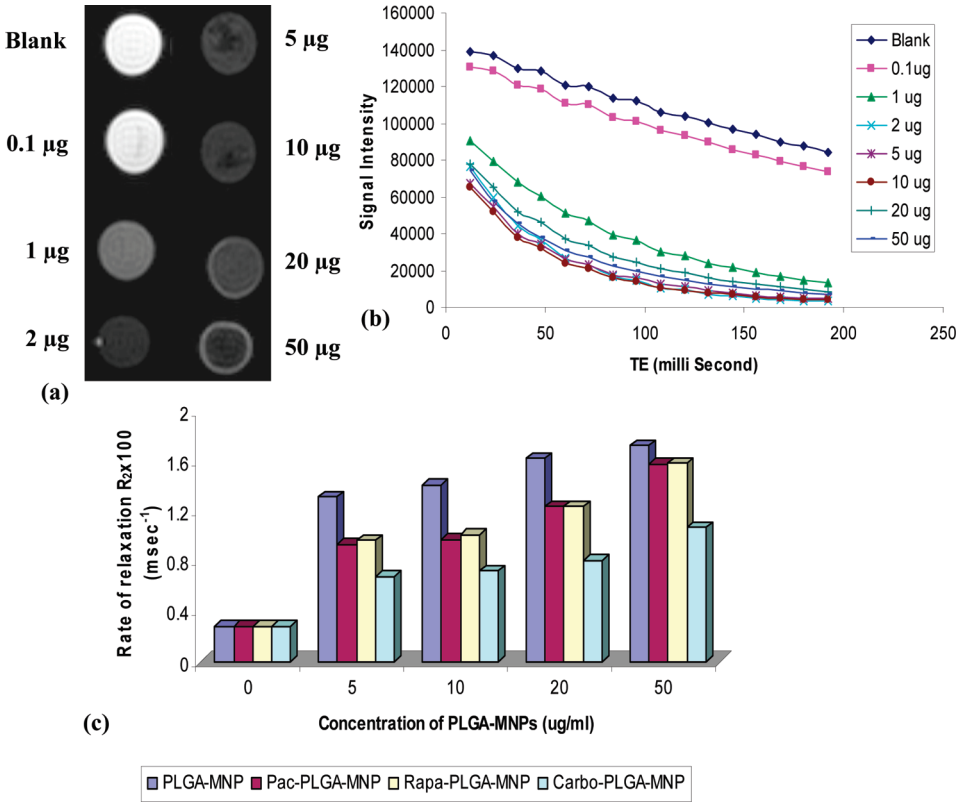

Figure 4. (a) MR signal intensity of PLGA-MNPs in a phantom agar gel at various iron concentrations. Blank phantom agar gels were taken as controls. (b) T_2 relaxation analysis curves of PLGA-MNPs in a phantom agar gel at different concentrations (data as mean intensity within the region of interest (ROI)). (c) T_2 relaxation rate (R_2) of different formulations of PLGA-MNPs.

blood was calculated from the graph of the signal intensity vs time (min), which appeared to be ~47 min (Figure 5a).

3.7. *In Vivo* MRI. The *in vivo* MRI experiments of the liver were carried out on rats. RARE T_2 weighted images in the axial plane of the normal rat liver at the baseline and immediately after injection of the PLGA-MNPs into rats were acquired; MR images acquired at various time points showed a gradual decrease in signal intensity and, at 24 h, a complete loss of the MR signal in the liver (signal void). This may be due to accumulation of the particles in the liver up to 24 h, indicating utilization of the PLGA-MNPs. However, there was an increase in signal intensity after 48 h of injection, but the strength of the signal intensity did not reach normal values, signifying the delayed clearance of the PLGA-MNPs from the body (Figure 5b,c)

3.8. Antibody Conjugation and Cellular Uptake. The human epidermal growth factor receptor (HER2) is overexpressed by cancer cells, so it was used as a tumor targeting marker for the treatment of metastatic cancer.[41] The conjugation efficiency of HER2 to PLGA-MNPs was ~74%, i.e., 0.7 μg/mg of particles, which was confirmed by protein estimation through a micro-BCA assay (data not shown).[21] To determine the change of the surface charge mediated by antibody conjugation to the surface of PLGA-MNPs, we measured the ζ potential and found a change from −23 mV (PLGA-MNPs) to about −19 mV (HER2- PLGA-MNPs). To test the uptake through receptor-mediated endocytosis, we have used MCF-7 cells. The uptake efficiency of HER2 conjugated nanoparticles was determined using an MNP assay and a fluorescence method. Earlier experimental studies in our lab and elsewhere have established 6-coumarin to be a useful probe for the uptake studies of nonfluorescent drug-loaded nanoparticles.[32,40,42]

The MNP assay was done on the basis of the amount of Fe_3O_4 per milligram of protein that was taken up by the cells. It was revealed that the cellular uptake of HER2-PLGA-MNPs was ~3 times more as compared to unconjugated PLGA-MNPs (Figure 6a). To validate the higher uptake due to the presence of HER2 conjugated to the nanoparticles, a competitive inhibition assay was performed by adding different concentrations of native HER2 along with the nanoparticles. The result revealed that the native HER2 antibody acts as a competitive inhibitor for the uptake of HER2 conjugated PLGA-MNPs (Figure 6a). The fluorescence spectroscopy results of the intracellular uptake studies on MCF-7 cells showed that HER2 conjugated 6-coumarin-loaded PLGA-MNPs were internalized at a rate ~3 times higher than that of unconjugated 6-coumarin-loaded PLGA-MNPs and ~6 times higher than that of the native 6-coumarin (Figure 6b), which was in accordance with MNP assay observations. To further confirm the internalization of the 6-coumarin-loaded PLGA-MNPs and to visualize the fate of the nanoparticles, the native 6-coumarin, 6-coumarin-loaded PLGA-MNPs, and HER2 conjugated 6-coumarin-loaded PLGA-MNP treated MCF-7 cells were studied under confocal microscopy (Figure 6c).

But, the nanoparticle formulations get trapped inside the cells, and with time the fluorescence intensity gradually increases. The HER2 conjugated nanoparticles have more fluorescence intensity than unconjugated nanoparticles due to higher uptake through the receptor-mediated endocytosis because of the presence of HER2 receptors on the cell surface.[30]

3.9. Antiproliferative Assay. The PLGA-MNPs are efficient in delivering both hydrophobic and hydrophilic drugs to the cancer cells. The therapeutic efficacies of different native drug,

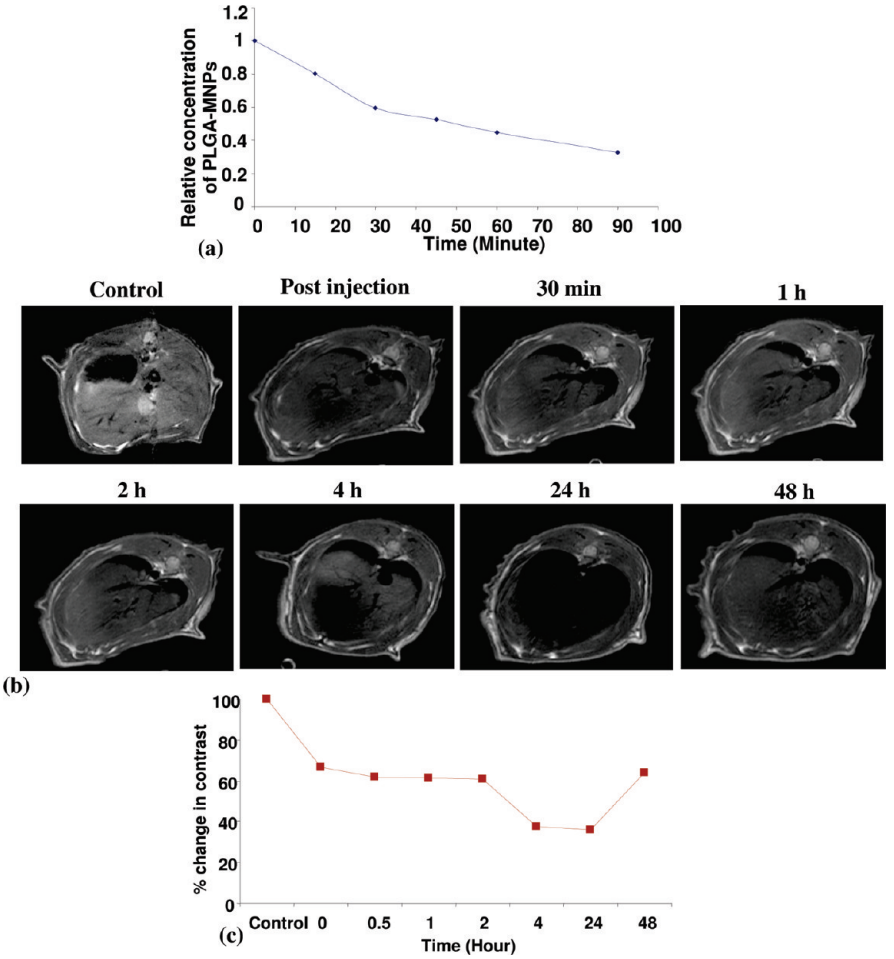

Figure 5. (a) Circulation half-life of PLGA-MNPs in a rat obtained after intravenous injection of the PLGA-MNPS (dose, 7 mg/kg body weight of rat). (b) The magnetic resonance imaging signal trend in the liver obtained after intravenous injection of the PLGA-MNPS (dose, 7 mg/kg body weight of rat). The axial section of the liver were taken at various designated time. (c) Time course of magnetic resonance imaging contrast signal in the liver after intravenous injection of the PLGA-MNPs into two different rats.

drug-loaded PLGA-MNP, and HER2 conjugated drug-loaded PLGA-MNP formulations were investigated using a reagent based cytotoxicity assay[30] in the MCF-7 and PANC-1 cell lines. Both the cancer cell lines showed a typical dose-dependent sigmoidal antiproliferative effect (Supporting Information). The half maximal inhibitory concentration (IC_{50}) is the quantitative measurement for the cytotoxic effect *in vitro*. IC_{50} values were calculated from the obtained sigmoidal curves of each drug formulation on both cell lines, and the results demonstrated that the HER2 conjugated drug-loaded PLGA-MNPs showed higher antiproliferative activity than unconjugated drug-loaded PLGA-MNPs and the native drug (Table 3).

In MCF-7 cells (Supporting Information, Figure S4), the IC_{50} values (Table 3) suggest that the HER2 conjugated paclitaxel-loaded PLGA-MNPs are ~12 times more effective than native paclitaxel and ~2 times more effective than paclitaxel-loaded PLGA-MNPs. Similarly, in the case of rapamycin, the HER2 conjugated PLGA-MNPs are ~10 times more effective than native drugs. In our combined drug formulation (paclitaxel + rapamycin), the HER2 conjugated nanoparticles are ~46 times more effective than combined native drugs and ~10 times more effective than unconjugated combined drug-loaded PLGA-MNPs. In addition, the HER2 conjugated carboplatin-loaded PLGA-MNPs are ~36 times more effective than native carboplatin and ~5 times more effective than carboplatin-loaded unconjugated PLGA-MNPs. In the combined drug formulation (paclitaxel + carboplatin), the HER2 conjugated nanoparticles are ~14 times more effective than combined native drugs and ~3 times more effective than unconjugated combined drug-loaded PLGA-MNPs.

In PANC-1 cells (Supporting Information, S4), the IC_{50} values (Table 3) suggest that the HER2 conjugated paclitaxel-loaded PLGA-MNPs are ~5 times more effective than native paclitaxel and ~2 times more effective than unconjugated paclitaxel-loaded PLGA-MNPs. In the case of rapamycin, the HER2 conjugated PLGA-MNPs are ~10 times more effective than the native drug and ~6 times more effective than unconjugated rapamycin-loaded PLGA-MNPs. In our combined drug formulation (paclitaxel + rapamycin), the HER2 conjugated nanoparticles are ~203 times more effective than native combined drugs and ~19 times more effective than unconjugated combined drug-loaded PLGA-MNPs. In addition, the HER2 conjugated carboplatin-loaded PLGA-MNPs are ~90 times more effective than native carboplatin and ~2 times more effective than unconjugated carboplatin-loaded PLGA-MNPs. In the combined drug formulation (paclitaxel + carboplatin), the HER2 conjugated PLGA-MNPs are ~10 times more effective than native combined drugs and ~5 times more effective than unconjugated combined drug-loaded PLGA-MNPs.

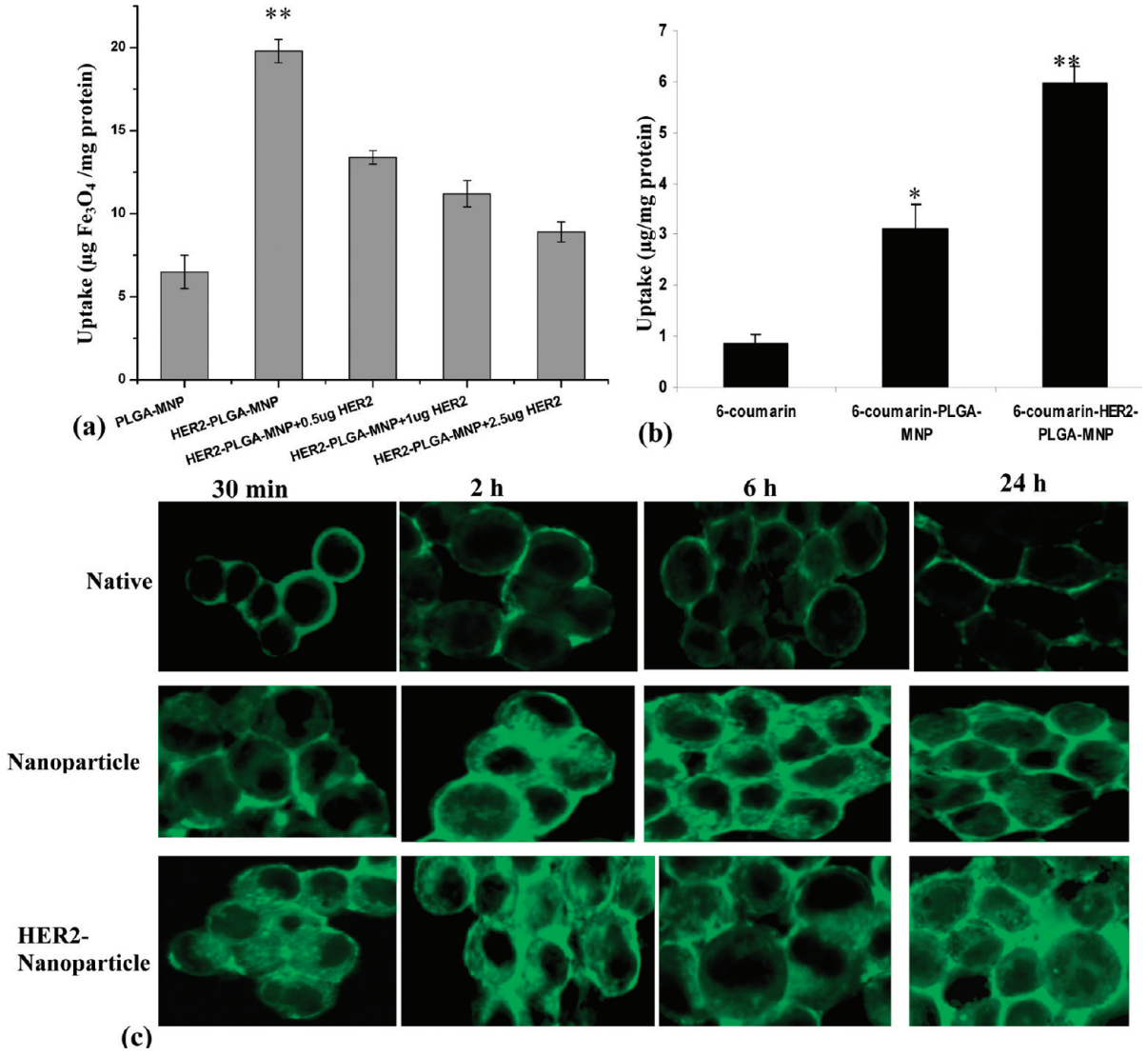

Figure 6. (a) Quantitative uptake of PLGA-MNPs in MCF-7 cells by MNP assay. Data as mean ± SEM, $n = 6$, (**) $p < 0.005$. (b) Quantitative intracellular uptake of 6-coumarin, 6-coumarin-loaded PLGA-MNPs, and HER2 conjugated 6-coumarin-loaded PLGA-MNPs in MCF-7 cells. Data as mean ± SEM, $n = 6$, (**) $p < 0.005$ and (*) $p < 0.05$. (c) Confocal fluorescence images showing time-dependent intracellular uptake of 6-coumarin, 6-coumarin-loaded nanoparticles, and HER2 conjugated 6-coumarin-loaded nanoparticles in MCF-7 cells.

3.10. Mitochondrial Membrane Potential Analysis. The loss of mitochondrial membrane potential is one of the features of the apoptotic pathway. JC-1 is a dye that forms either J-aggregates or monomers, depending on the state of the mitochondrial membrane potential, with the emissions of the two dye forms detectable by flow cytometry at 585 or 530 nm, respectively.[43] The study of mitochondrial membrane potential in both MCF-7 (Figure 7a) and PANC-1 (Figure 7b) cells, using JC-1 dye in a flow cytometry analysis, showed that drug-loaded nanoparticles showed the prevention of formation of JC aggregates other than native drugs, indicating a loss of $\Delta\Psi m$. In addition, the HER2 conjugated drug-loaded nanoparticles showed a greater loss in membrane potential, which is due to the higher uptake by the cells. Furthermore, the synergistic effect of dual drug formulation also is visible in the JC-1 data. The combined drug formulations show a greater loss in membrane potential and less JC aggregate formation, thus activating more apoptosis. In the JC-1 results, the upper right quarter indicated the viable population, and the lower right quarter indicates the apoptotic cell population. Our results revealed that the percentage of the viable population is lower in the case of the HER2 conjugated drug-loaded PLGA-MNPs than that of unconjugated drug-loaded PLGA-MNPs and the native drug treated cells in both cell lines (MCF-7 and PANC-1).

In MCF-7, the HER2 conjugated drug-loaded PLGA-MNPs showed only ~13% apoptotic population for single drug formulation and ~28% apoptotic population for dual drug formulation. In PANC-1, the HER2 conjugated drug-loaded PLGA-MNPs showed ~40% apoptotic population for single drug formulation and ~55% apoptotic population for dual drug formulation. Thus, the HER2 conjugated dual-drug-loaded PLGA-MNPs showed the highest apoptotic cell populations, showing the effectiveness of the formulation in the cancer cell lines. Further, while comparing the two different HER2 conjugated dual drug formulations, it could be revealed that the paclitaxel + rapamycin drug combination is more effective than the paclitaxel + carboplatin drug formulation in the case of MCF-7 and PANC-1 cell lines.

3.11. Western Blot Analysis. Different drugs initiated their respective apoptotic pathways. Therefore, to determine the molecular mechanism of the apoptotic pathways, Western

Table 3. IC_{50} Values of Different Native Drugs, Drug-Loaded PLGA-MNPs, and HER2 Conjugated Drug-Loaded PLGA-MNPs

	IC_{50} values (ng/mL)	
sample	MCF-7	PANC-1
native paclitaxel	27.6	9.46
paclitaxel PLGA-MNP	4.01	3.8
paclitaxel-HER2-PLGA-MNP	2.2	1.96
native rapamycin	123.5	71.3
rapamycin PLGA-MNP	28.9	43.90
rapamycin-HER2-PLGA-MNP	12.3	7.51
native (pac + rapa)	37.4	12.23
(Pac + rapa)-PLGA-MNP	3.81	1.15
(Pac + rapa)-HER2-PLGA-MNP	0.08	0.06
native carboplatin	10279	809
carboplatin PLGA-MNP	1539	19.3
Carboplatin-HER2-PLGA-MNP	278.6	9.2
native (pac + carbo)	28.11	15.42
(Pac + carbo)-PLGA-MNP	6.02	0.99
(Pac + carbo)-HER2-PLGA-MNP	2.03	0.19

blotting of different proteins (Figure 8) was done. It is evident from the previous apoptotic studies that the HER2 conjugated drug-loaded PLGA-MNPs were more effective in inducing apoptosis than unconjugated drug-loaded PLGA-MNPs. Thus, in Western blot experiments, we have compared the native drug treated cells only with the HER2 conjugated PLGA-MNPs.

Paclitaxel hyperpolarizes the microtubules of the cells and induces apoptosis.[44] So, after treatment with paclitaxel, the level of proapoptotic protein p53 increased, which in turn induces another proapoptotic protein p21. From the results, it can be revealed that the levels of p53 and p21 are higher in the case of HER2-paclitaxel-PLGA-MNPs than that of native paclitaxel (Figure 8a,b). Similarly, rapamycin initiates apoptosis by inactivating the mTOR pathway and the subsequent downstream proteins like p70S6K1.[45] From this result (Figure 8a), it can be observed that the rapamycin treated cells showed a decreased expression of p70S6K1 relative to that of control cells.

The decrease in the expression of p70S6K1 is higher in the case of HER2 conjugated rapamycin-loaded PLGA-MNPs than the unconjugated PLGA-MNPs. The decreased expression of p70S6K1 can also be visible in the case of the combined drug formulation (paclitaxel + rapamycin). In the case of rapamycin, the levels of proapoptotic proteins like p53 and p21 also get increased. This can be evident from the resulting banding pattern (Figure 8a). The drug carboplatin intercalates between the DNA double helix and induces apoptosis by phosphorylating the γ-H2AX histone protein.[46] So, the increase in the intensity of the p-γ-H2AX can be visible in the case of carboplatin-treated cells or the combined drug (paclitaxel + carboplatin) treated cells. In addition, the HER2 conjugated carboplatin-loaded PLGA-MNPs show higher phosphorylation of γ-H2AX than that of the native drug, showing the effectiveness of the formulation (Figure 8b). Also, in the case of carboplatin treated cells, the p53 and the p21 protein levels get increased, as these are the downstream proteins of the apoptotic pathway (Figure 8b). Further, in the case of both combined drug formulations, the levels of p53 and p21 are higher than those of individual drug formulations (Figure 8a). The combined drug formulations showed a synergistic effect for both the drugs. This might be due to the activation of two apoptotic signaling pathways relating to two different drugs (Figure 8c).

Thus, to emphasize the synergistic effect of the combined drug formulations, the effect of drug treatment on a late apoptotic protein poly(ADP-ribose) polymerase (PARP-1) was studied. The cleavage of the PARP-1 protein takes place when there is apoptosis.[47] In the native drug treated cells, this cleavage was not observed; however, there is a slight decrease in the intensity of the band of uncleaved PARP-1 when compared with the control cells. The HER2 conjugated PLGA-MNP treated cells illustrated the cleavage of PARP-1. Moreover, the cleavage of PARP-1 was significant in the case of the HER2 conjugated combined drug-loaded PLGA-MNPs at a given concentration (0.01 μg/mL), even at 24 h (Figure 8a,b).

4. DISCUSSION

A magnetically targeted drug delivery system has remarkable potentiality for the precise delivery of chemotherapeutic drugs along with the advantage of being used as a contrast agent for MRI. While discussing the therapeutic aspect of the magnetic nano vehicle in relation to cancer therapy, combinational drug delivery provides an effective modality to treat cancer cells due to the synergistic action of different drugs. This synergistic action of drugs is the result of diverse mechanisms of action of different drugs. Polymer-coated magnetic nanoparticles play a major role in delivering combined chemotherapeutics with reduced systemic toxicity, by establishing the stability and routing the particles to different targeted sites in the body. This also provides a longer blood half-life after administration *in vivo* primarily that depends on the physicochemical properties of drug-loaded MNPs such as size, morphology, charge, and surface chemistry.[48] The excellent spheroid and discrete morphology, average hydrodynamic size of ~240 nm, and high ζ potential (−23 mV) of the formulated PLGA-MNPs demonstrated characteristic features of a highly stable nanocarrier, which could escape from the RES, thereby preventing their uptake by macrophages.[30,48] The magnetization measurement provided by the SQUID for the PLGA-MNPs (~ 29 emu/g) is quite good enough to be dragged by an external magnetic field. Similar kinds of magnetization values were also reported by Liu et al. and Yang et al. working on PLGA coated magnetite particles.[29,49]

To establish a combined drug delivery vehicle, however, the major challenge faced is to load different drugs having dissimilar physical properties into the same carrier. In addition, for the effective cancer treatment, the drug delivery vehicle should carry the heavy payload so that it can systemically and effectively dissociate the drugs to the affected tissues. Apparently, in our PLGA-MNP formulation, we have achieved ~82% entrapment for hydrophobic drugs in individual paclitaxel and rapamycin formulations and also in the combined paclitaxel+rapamycin/paclitaxel+carboplatin formulation. Hydrophilic drug carboplatin showed ~47% entrapment in both individual and combined formulations. Co-delivery of both hydrophobic and hydrophilic drugs is a challenging task. Zhang et al. have encapsulated hydrophobic docetaxel and hydrophilic doxorubicin in an approximately 9:1 molar ratio.[18] But, such a ratio could not help to achieve the advantages related to the co-delivery of multiple drugs. We have encapsulated the hydrophobic paclitaxel and hydrophilic carboplatin in PLGA-MNPs with a ~2:1 ratio. Furthermore, the effective cytotoxicity effect of the drugs primarily depends on the release behavior of the encapsulated drugs

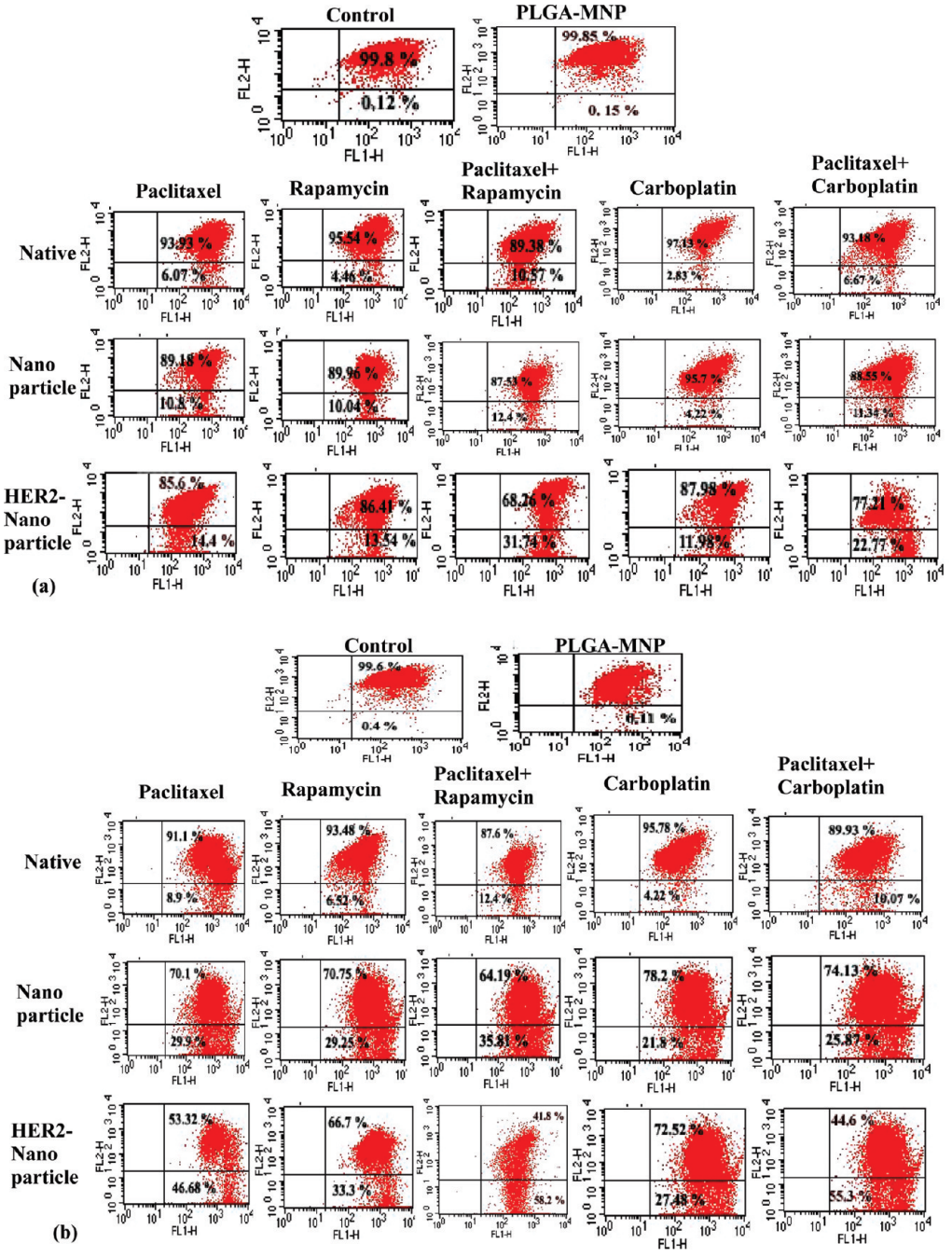

Figure 7. (a) Changes in mitochondrial membrane potential measured through JC-1 dye after 24 h of treatment with the native drug and different drug formulations (100 ng/mL) in MCF-7 cells. (b) Changes in mitochondrial membrane potential measured through JC-1 dye after 24 h of treatment with the native drug and different drug formulations (100 ng/mL) in PANC-1 cells.

in vitro. The sustained release of drugs from the nanoparticles is an essential requirement for cancer therapy.[14] The amorphous state of the entrapped drug inside the PLGA-MNPs (confirmed by DSC analysis) is further attributed to the sustained release activity of the drug. The drug-loaded PLGA-MNPs showed a sustained release of ~85% of the drug in three weeks.

To further increase the efficiency of dual drug system, ligand/receptor-mediated targeting has emerged as a novel paradigm in the area of active targeting.[41] The conjugation of nanoparticulate drug carriers with a ligand leads toward selective targeting of the cancerous cells, thereby focusing drug delivery augmented by the enhanced permeability and retention (EPR) effect.[50] As a step to address this issue, efforts are directed for improved drug-loaded PLGA-MNP, conjugated with HER2 antibodies against the HER2/neu receptors overexpressed in numerous cancer tissues.

The combined drug delivery system having an active targeting ligand provides an opportunity to exercise a lower dose of the drug to minimize toxicity toward healthy cells. The cytotoxic effect of different drug-loaded PLGA-MNP formulations determined by a cytotoxicity assay showed a typical dose-dependent sigmoidal antiproliferative effect on both MCF-7 and PANC-1 cell lines. The HER2 conjugated PLGA-MNPs showed a greater

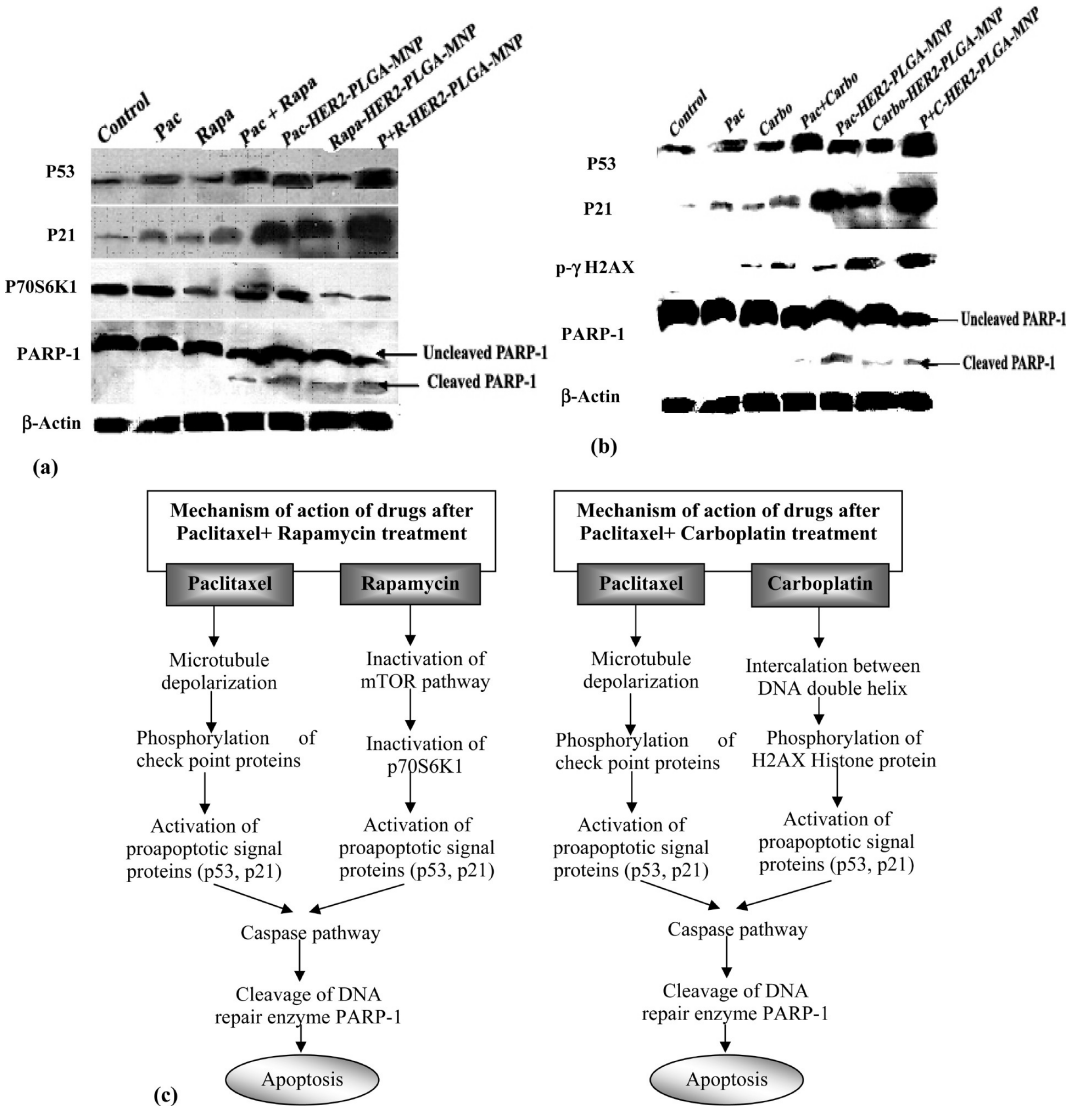

Figure 8. (a) Immuno-blot analysis of MCF-7 cells treated with 100 nM/mL of native paclitaxel (Pac), native rapamycin (Rapa), native paclitaxel + rapamycin (Pac + rapa), paclitaxel-HER2-PLGA-MNPs (Pac-HER2-PLGA-MNP), rapamycin-HER2-PLGA-MNP (Rapa-HER2-PLGA-MNP), and paclitaxel + rapamycin-HER2-PLGA-MNP (P + R-HER2-PLGA-MNP). (b) Immuno-blot analysis of MCF-7 cells treated with 100 nM/mL of native paclitaxel (Pac), native carboplatin (Carbo), native paclitaxel + carboplatin (Pac + carbo), paclitaxel-HER2-PLGA-MNPs (Pac-HER2-PLGA-MNP), carboplatin-HER2-PLGA-MNP (Carbo-HER2-PLGA-MNP), and paclitaxel + carboplatin-HER2-PLGA-MNP (P + C-HER2-PLGA-MNP). (c) Schematic diagram of the mechanism of action of drugs giving rise to a synergistic effect in combined drug formulations.

cytotoxic effect than that of the unconjugated PLGA-MNPs. In addition, the combination drug therapy resulted in lower IC_{50} values. This higher cytotoxicity may be due to the synergistic antiproliferative effect of dual drugs in a targeted manner. Similar synergistic effects of dual-drug-loaded MNPs were reported by Dilnawaz et al. and Jain et al.[21,22]

The cytotoxicity caused by the treatment of drug formulations can either lead to necrotic or apoptotic cell death. During apoptosis, the mitochondrial permeability transition pores located in the inner mitochondrial membrane get opened up[51,52] and permit redistribution of the molecules across the inner mitochondrial membrane, which leads to the loss of mitochondrial membrane potential.[53,54] The cells treated with drug-loaded PLGA-MNPs revealed a higher apoptotic population than that of the native drug due to the accumulation and sustained release of the drug from the nanoparticles. Further, HER2 conjugated drug-loaded PLGA-MNPs demonstrated a higher percentage of JC monomer population due to enhanced uptake of the conjugated PLGA-MNPs. In addition, the combined drug formulations achieved a synergistic effect of different drugs. Further, the apoptosis study using Annexin-V supplemented this result. The synergistic effect shown by dual-drug-loaded PLGA-MNPs might be due to the activation of two apoptotic pathways related to the two different drugs.

The effectiveness of the drug-loaded targeted PLGA-MNP formulations compared to those of the native drug were also noticeable from the chosen apoptotic pathway related cell protein in a Western blot analysis. Paclitaxel is a chemotherapeutic agent that disrupts microtubule dynamics by hyperpolarization and causes subsequent mitotic arrest and apoptotic cell death by inducing the level of proapoptotic proteins p53 and p21.[44] The drug rapamycin is an immunosuppressant and serine/threonine kinase inhibitor belonging to the class of mammalian targets of rapamycin (mTOR) with a signaling pathway that

phosphorylates ribosomal protein p70S6 kinase (p70S6K1) and translation repressor protein (4E-BP1), resulting in the transcription of critical mRNAs involved in cell cycle progression from G1 to the S phase.[55] Rapamycin decreases the phosphorylation of p70S6K1 and 4E-BP1, causing G1 arrest. Further, carboplatin is a chemotherapeutic drug that intercalates in the DNA double helix. After intercalation of the drug in the DNA double helix, the γ-H2AX histone protein gets phosphorylated. So, as the damage to the DNA increases, the level of p-γ-H2AX gets increased, and the cell cycle arrests at the G2/M phase.[46] In the combined paclitaxel and rapamycin formulation, inactivation of the mTOR pathway and the microtubule damage occurred simultaneously, causing the activation of the apoptotic pathway. Similarly, the combined carboplatin and paclitaxel formulation initiated apoptosis by both intercalation in the DNA helix and depolarization of the microtubule assembly simultaneously. The synergistic effects of both drugs were visible during PARP-1 protein expression. PARP-1 cleavage is one of the indicators of late apoptosis, inducing a mitochondrial death pathway.[47] The cleavage of the PARP-1 protein was not observed with a single drug treatment (100 ng/mL). However, at 100 ng/mL, the combined drug formulations demonstrated PARP-1 cleavage. Our experimental outcomes revealed that a single drug delivery system was not able to fulfill the appropriate level of apoptosis necessary to kill the cancer cells, which can be achieved with a targeted dual drug delivery system. As a holistic approach, our results suggested that combined drug-loaded HER2-PLGA-MNPs provided an effective indication for the therapeutic aspects of cancer therapy.

Another role of these magnetic nanoparticles is its use as a contrast agent for MRI. The biodegradable polymer-coated MNPs (PLGA-MNPs) function as image contrast agents due to shortening T_2 relaxation. In comparison with the commercial iron oxide particles like Feridex IV or Resovist, the formulated PLGA-MNPs showed a better contrast effect due to higher T_2 relaxivity. The dextran-coated Feridex IV showed a hydrophilic nature and allowed the particles to remain in the closer proximity of water molecules, which might have led to shortening of T_1.[22] Further, while comparing the T_2 relaxivity behavior of drug-loaded PLGA-MNPs with that of void PLGA-MNPs, the relaxivity marginally decreased after drug loading but still appears to be a better candidate than the commercial ones. The hydrophobic drug-loaded PLGA-MNPs showed higher T_2 relaxivity than that of the hydrophilic drug-loaded PLGA-MNPs. This may probably be due to the fact that the hydrophobic drugs decreased the hydrophilicity of MNPs while the hydrophilic drug-like carboplatin helped in increasing the T_1.

Regarding the blood circulation half-life of the nanoparticles, Feridex IV has a half-life of only 4.6 min.[22] Jain et al.[22] developed a pluronic coated hydrophilic magnetic nanoparticle, which demonstrated a blood circulation half-life of around 31.2 min in athymic nude mice. In another study, Mejias et al. formulated DMSA-coated iron oxide nanoparticles which showed a blood half-life of 15 min in Wistar rats.[56] Our formulated PLGA-MNPs showed a blood half-life of ~45 min in Wistar rats. As found in the literature, we are the first group to report a formulation that shows a higher blood circulation time, which could help as an efficient carrier for drug delivery and simultaneous imaging.

As the liver is the vital organ playing a major role in metabolism, the use of PLGA-MNPs in the liver was studied by MR imaging. The PLGA-MNPs of size ~240 nm can easily enter the organ through the sinusoidal or discontinuous capillaries, which has large endothelial openings (>1000 nm diameter). Thus, after intravenous injection in the tail vein of Wistar rats, the formulated PLGA-MNPs accumulated in the liver after 15 min. The MR signal intensity in the liver gradually decreased up to 24 h. However, after 48 h, the MR signal intensity gradually increased, indicating clearance of the PLGA-MNPs from the system. Recently, Prashant et al.[57] has developed iron-oxide-loaded polylactic acid and α-tocopherol polyethylene glycol 1000 succinate (TPGS) nanoparticles and reported the imaging features and clearance of the nanoparticles in the liver. They found that the iron oxide TPGS nanoparticles were cleared from the liver within 24 h. Our formulated PLGA-MNPs showed an enhanced circulation and residence time in the liver up to 24 h with gradual clearance thereafter. Therefore, the developed PLGA-MNPs with increased circulation and retention time in the liver may act as an effective drug delivery system that can easily be monitored through MR imaging. We hypothesize that the drug-loaded PLGA-MNPs would facilitate the therapeutics and continuous monitoring of the cancer tissues due to the defective tumor vasculature and the EPR effect.[58]

5. CONCLUSION

The formulated drug-loaded PLGA-MNPs were characterized and assessed for efficacy and suitability in guided drug delivery systems as well as use in MRI as contrast agents. The formulated drug carrier system of PLGA-MNP provided the opportunity to deliver both hydrophobic and hydrophilic drugs either alone or in combination in a sustained release manner, substantiating dose-dependent cytotoxic activity in MCF-7 and PANC-1 cells. The conjugation of HER2 on the surface of the PLGA-MNPs furnished the possibility of co-delivery of single or multiple drugs toward active targeting with an increased synergistic therapeutic index. Thus, the results suggest that the use of antibody conjugated polymer-coated magnetic nanoparticles could be applicable as a progressive therapeutic tool for targeted cancer therapy. In addition, the PLGA-MNPs were evaluated as effective contrast agents, which could contribute to potentiate drug delivery and imaging aspects in cancer therapy.

■ ASSOCIATED CONTENT

Ⓢ Supporting Information. Further details of the materials, methodology of different physicochemical characterizations, quantification of drug entrapment, release kinetics study, uptake study, apoptosis study using Annexin V, results of FT-IR, release kinetics, apoptosis study, and figure of antiproliferative effect of different drugs. This information is available free of charge via the Internet at http://pubs.acs.org.

■ AUTHOR INFORMATION

Corresponding Author

*Phone: 91-674-2302094. Fax: 91-674-2300728. E-mail: sanjeebsahoo2005@gmail.com.

Author Contributions

§Both authors have equal contribution.

■ REFERENCES

(1) Hafeli, U. O. *Int. J. Pharm.* **2004**, *277*, 19–24.

(2) Ito, A.; Takizawa, Y.; Honda, H.; Hata, K.-I.; Kagami, H.; Ueda, M.; Kobayashi, T. *Tissue Eng.* **2004**, *10*, 833–840.

(3) Mahmoudi, M.; Simchi, A.; Imani, M.; Shokrgozar, M. A.; Milani, A. S.; Hafeli, U. O.; Stroeve, P. *Colloids Surf. B* **2009**, *75*, 300–9.

(4) Alexiou, C.; Schmidt, A.; Klein, R.; Hulin, P.; Bergemann, C.; Arnold, W. *J. Magn. Magn. Mater.* **2002**, *252*, 363–366.

(5) Polyak, B.; Friedman, G. *Expert Opin. Drug Delivery* **2009**, *6*, 53–70.
(6) Lubbe, A.; Alexiou, C.; Bergemann, C. *J. Surg. Res.* **2001**, *95*, 200–206.
(7) Briley-Saebo, K.; Bjørnerud, A.; Grant, D.; Ahlstrom, H.; Berg, T.; Kindberg, G. M. *Cell Tissue Res.* **2004**, *316*, 315–23.
(8) Stark, D. D.; Weissleder, R.; Elizondo, G.; Hahn, P. F.; Saini, S.; Todd, L. E.; Wittenberg, J.; Ferrucci, J. T. *Radiology (Oak Brook, IL, U. S.)* **1988**, *168*, 297–301.
(9) Weissleder, R.; Bogdanov, A.; Neuwelt, E. A.; Papisov, M. *Adv. Drug Delivery Rev.* **1995**, *16*, 321–24.
(10) Corot, C.; Robert, P.; Idée, J. M.; Port, M. *Adv. Drug Delivery Rev.* **2006**, *58*, 1471–1504.
(11) Butoescu, N.; Seemayer, C. A.; Palmer, G.; Guerne, P.; Gabay, C.; Doelker, E.; Jordan, O. *Arthritis Res. Ther.* **2009**, *11*, 1–10.
(12) Lee, S. J.; Jeong, J. R.; Shin, S. C.; Kim, J. C.; Chang, Y. H.; Lee, K. H.; Kim, J. D. *Coll. Surf., A* **2005**, *255*, 19.
(13) Okassa, L.; Marchais, H.; Douziech-Eyrolles, L.; Hervé, K.; Cohen-Jonathan, S.; Munnier, E.; Soucé, M .; Linassier, C.; Dubois, P.; Choupra, I. *Eur. J. Pharm. Biopharm.* **2007**, *67*, 31–38.
(14) Sahoo, S. K.; Labhasetwar, V. *Drug Discovery Today* **2003**, *8*, 1112–1120.
(15) Yang, J.; Park, S.; Yoon, H.; Huh, Y.; Haam, S. *Int. J. Pharm.* **2006**, *324*, 185–190.
(16) Qiu, L.; Bae, Y. *Biomaterials* **2007**, *28*, 4132–42.
(17) Wei, L.; Cai, C.; Lin, J.; Chen, T. *Biomaterials* **2009**, *30*, 2606–2613.
(18) Zhang, L.; Radovic-Moreno, A. F.; Alexis, F.; Gu, F. X.; Basto, P. A.; Bagalkot, V.; Jon, S.; Langer, R. S.; Farokhzad, O. C. *ChemMedChem* **2007**, *2*, 1268–1271.
(19) Mitragotri, S. *Pharm. Res.* **2000**, *17*, 1354–1359.
(20) Walsh, C. *Nature* **2000**, *406*, 775–781.
(21) Dilnawaz, F.; Singh, A.; Mohanty, C.; Sahoo, S. K. *Biomaterials* **2010**, *31*, 3694–3706.
(22) Jain, T. K.; Richey, J.; Strand, M.; Leslie-Pelecky, D. L.; Flask, C. A.; Labhasetwar, V. *Biomaterials* **2008**, *29*, 4012–21.
(23) Lee, B.-J.; Ryu, S.-G.; Cui, J.-H. *Int. J. Pharm.* **1999**, *188*, 71–80.
(24) Aryal, S.; Hu, C. M.; Zhang, L. *Small* **2010**, *6*, 1442–8.
(25) Yang, J.; Lee, H.; Hyung, W.; Park, S.-S.; Haam, S. *J. Microencapsulation* **2006**, *23*, 203–212.
(26) Bulte, J. W.; Hoekstra, Y; Kamman, R. L; Magin, R. L; Webb, A. G.; Briggs, R. W; Go, K. G.; Hulstaert, C. E.; Miltenyi, S; The, T.; Leij, L. *Magn. Reson. Med.* **1992**, *25*, 148–157.
(27) Tiefenauer, L.; Kuhne, G.; Andres, R. *Bioconjugate Chem.* **1993**, *4*, 347–52.
(28) Artemov, D.; Mori, N.; Okollie, B.; Bhujwalla, Z. *Magn. Reson. Med.* **2003**, *49*, 403–408.
(29) Liu, X.; Kaminski, M.; Chen, H.; Torno, M.; Taylor, L.; Rosengart, A. J. *Controlled Release* **2007**, *119*, 52–58.
(30) Acharya, S.; Dilnawaz, F.; Sahoo, S. K. *Biomaterials* **2009**, *30*, 5737–5750.
(31) Jain, T. K.; Morales, M. A.; Sahoo, S. K.; Leslie-Pelecky, D. L.; Labhasetwar, V. *Mol. Pharmaceutics* **2005**, *2*, 194–205.
(32) Panyam, J.; Sahoo, S. K.; Prabha, S.; Labhasetwar, V. *Int. J. Pharm.* **2003**, *262*, 1–11.
(33) Mosmann, T. *J. Immunol. Methods* **1983**, *65*, 55–63.
(34) Raffaella, A.; Simona, R.; Rosanna, P.; Rita, B.; Annalisa, L.; Vincenzo, P.; Salvatore, V.; Romano, M. F. *Blood* **2005**, *106*, 1400–1406.
(35) Misra, R.; Acharya, S; Dilnawaz, F.; Sahoo, S. K. *Nanomedicine (London, U.K)* **2009**, *4*, 519–30.
(36) Kim, J.; Lee, J. E.; Lee, S. H.; Yu, J. H.; Lee, J. H.; Park, T. G.; Hyeon, T. *Adv. Mater. (Weinheim, Ger.)* **2008**, *20*, 478–483.
(37) Prabha, S.; Zhou, W. Z.; Panyam, J.; Labhasetwar, V. *Int. J. Pharm.* **2002**, *244*, 105–15.
(38) Guinier, A. *Diffraction in Crystals, Imperfect Crystals and Amorphous Bodies*; Dover Publications Inc: Mineola, NY,1963; p 378.
(39) Liu, X.; Kaminski, M. D.; Guan, Y.; Chen, H.; Liu, H.; Rosengart, A. J. *J. Magn. Magn. Mater.* **2006**, *306*, 248–253.
(40) Sahoo, S. K.; Ma, W.; Labhasetwar, V. *Int. J. Cancer* **2004**, *112*, 335–340.
(41) Das, M.; Mohanty, C.; Sahoo, S. K. *Expert Opin. Drug Delivery* **2009**, *6*, 285–304.
(42) Sahoo, S. K.; Labhasetwar, V. *Mol. Pharmaceutics* **2005**, *2*, 373–83.
(43) Cossarizza, A.; Baccarani-Contri, M.; Kalashnikova, G.; Franceschi, C. *Biochem. Biophys. Res. Commun.* **1993**, *197*, 40–45.
(44) Giannakakou, P.; Robey, R.; Fojo, T.; Blagosklonny, M. *Oncogene* **2001**, *20*, 3806–3813.
(45) Mondesire, W. H.; Jian, W.; Zhang, H.; Ensor, J.; Hung, M. C.; Mills, G. B.; Meric-Bernstam, F. *Clin. Cancer Res.* **2004**, *10*, 7031–42.
(46) Chiu, S.-J.; Yi-Jang Lee, Y.-J.; Hsu, T.-S.; Chen, W.-S. *Chem. Biol. Interact.* **2009**, *182*, 173–182.
(47) Dong, J.; Peng, J.; Zhang, H.; Mondesire, W.; Jian, W.; Mills, G.; Hung, M.-C.; Meric-Bernstam, F. *Cancer Res.* **2005**, *65*, 1961–1972.
(48) Gupta, A. K.; Gupta, M. *Biomaterials* **2005**, *26*, 3995–4021.
(49) Yang, J.; Lee, C.-H.; Park, J.; Seo, S.; Lim, E.-K.; Song, Y.; Suh, J.-S.; Yoon, H.; Huh, Y.-M.; Haam, S. *J. Mater.Chem.* **2007**, *17*, 2695–2699.
(50) Parveen, S.; Sahoo, S. K. *J. Drug Targeting* **2008**, *16*, 108–23.
(51) Kroemer, G.; Petit, P.; Zamzami, N.; Vayssiere, J.; Mignotte, B. *FASEB J.* **1995**, *9*, 1277–1287.
(52) Zamzami, N.; Susin, S.; Marchetti, P.; Hirsch, T.; Gómez-Monterrey, I.; Castedo, M.; Kroemer, G. *J. Exp. Med.* **1996**, *183*, 1533–44.
(53) Bernardi, P.; Petronilli, V. *J. Bioenerg. Biomembr.* **1996**, *28*, 131–138.
(54) Zoratti, M.; Szabo, I. *J. Bioenerg. Biomembr.* **1994**, *26*, 543–554.
(55) Meric, F.; Hunt, K. *Mol. Cancer Ther.* **2002**, *1*, 971–979.
(56) Mejías, R.; Pérez-Yagüe, S.; Roca, A.; Pérez, N.; Villanueva, Á.; Cañete, M.; Mañes, S.; Ruiz-Cabello, J.; Benito, M.; Amilcar, L.; Batlle, X.; Veintemillas-Verdaguer, S.; Morales, M. P.; Barber, D. F.; Serna, C. *J. Nanomedicine (London, U.K)* **2010**, *5*, 397–408.
(57) Prashant, C; Deepak, M.; Yang, C. T.; Chuang, K. H.; Jun, D.; Feng, S. S. *Biomaterials* **2010**, *31*, 5588–97.
(58) Maeda, H; Wu, J.; Sawa, T.; Matsumura, Y.; Hori, K. *J. Controlled Release* **2000**, *65*, 271–84.